

Supporting Information

ReO_x/TiO₂ – a recyclable solid catalyst for deoxydehydration

Lennart Sandbrink^[a], Elisabeth Klindtworth^[a], Husn-Ubayda Islam,^[b] Andrew M. Beale^[b,c] and Regina Palkovits^{[a]*}

[a] Institut für Technische und Makromolekulare Chemie (ITMC), RWTH Aachen University, Aachen, Germany

[b] Department of Chemistry, University College London, 20 Gordon Street, London, WC1H 0AJ, UK

[c] UK Catalysis Hub, Research Complex at Harwell, Rutherford Appleton Laboratories, Didcot, Oxon, OX11 0FA, UK

Email: palkovits@itmc.rwth-aachen.de

Table of contents:

1. General Experimental Section
2. Physisorption
3. TPR
4. ICP-OES
5. Hexanediol deoxydehydration
6. Comparison of reduction temperature for ReO_x/TiO₂
7. Recycling experiment at 190 °C
8. Hot filtration test
9. Mass transfer considerations
10. Reproducibility
11. Application to further substrates
12. XAFS
13. TEM-EDX
14. References

1. General Experimental Section

For synthesis of the supported catalysts, the appropriate amount of ammonium perrhenate as metal precursor was dissolved in ethanol (20 mL per gram support material) and subjected to a wet impregnation of the support materials. After removal of the solvent and drying at 120 °C over night, the catalysts were either stored under argon and used in catalysis or were further reduced in an H₂-atmosphere. For that, the catalysts were placed in a reduction oven, heated with a ramp of 2 K min⁻¹ to the desired temperature and held for 3 h under a constant stream of H₂. After cooling down, the oven was purged with argon and the final catalysts were stored under argon until further use.

In a typical reaction, a glass vessel (1.5 mL volume) was filled with 20 mg catalyst and 500 mg of a stock solution containing 20 mg 1,2-hexanediol, 15 mg mesitylene as internal standard and 3-octanol, a magnetic stir bar and sealed with a teflon lined screw cap. A metal jacket was preheated to the desired temperature, the vessel was placed inside and stirred with 700 rpm. The reaction time was started upon solvent reflux and stopped after the desired time by immersing into an ice bath. After filtration, the samples were analyzed via GC. For recycling experiments, the catalyst was separated via centrifuge (8000 rpm, 5 min), washed twice with fresh solvent and dried in an oven until reusing it. Reaction yields were determined by GC-FID analysis (Trace GC Ultra from Thermo Scientific) with use of a CP-SIL-Pona column.

Chemicals were used without further purification. Re (99,99%), Re₂(CO)₁₀ (98%), Re₂O₇ (99,9%), H₃CrReO₃ (98%) and ReO₃ (99,9%) were purchased from ABCR, ReO₂ (99,9%) from Alfa Aesar, NH₄ReO₄ (99,9%) and HReO₄ (40% Re solution) from Chempur, ethanol (>99,9%) from Chemsolute, 3-octanol (>97%), 1,2-hexanediol (98%) and mesitylene (99%) from Sigma. TiO₂ (ST61120), ZrO₂ (SZ31164), SiO₂ (SS61138) were kindly supplied by Saint-Gobain NorPro, Activated Carbon A SUPRA EUR was kindly supplied by Norit.

2. Physisorption

For characterization of porosity parameters, materials were activated in vacuo at 110 °C removing adsorbed molecules. The samples were measured using Quantachrome QuadraSorb and QuadraWin as evaluation software. Specific surface area was calculated using BET method in the range of p/p₀ = 0.05-0.3. Pore volume was calculated using total adsorbed volume at p/p₀ = 0.95. Material properties are depicted in table S1 and S2, the isotherms of the materials in figures S1 through S6.

Table S1. Properties of support material porosity determined by nitrogen physisorption.

Support Material	S _{BET} [m ² g ⁻¹]	V _P [cm ³ g ⁻¹]
TiO ₂	152	0.393
A SUPRA EUR	1879	0.966
ZrO ₂	105	0.288
SiO ₂	241	0.893

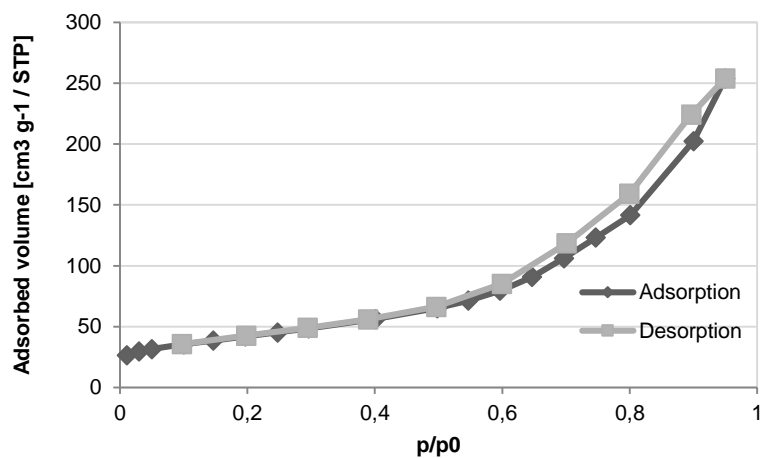


Figure S1. Nitrogen physisorption isotherm for Saint-Gobain TiO₂.

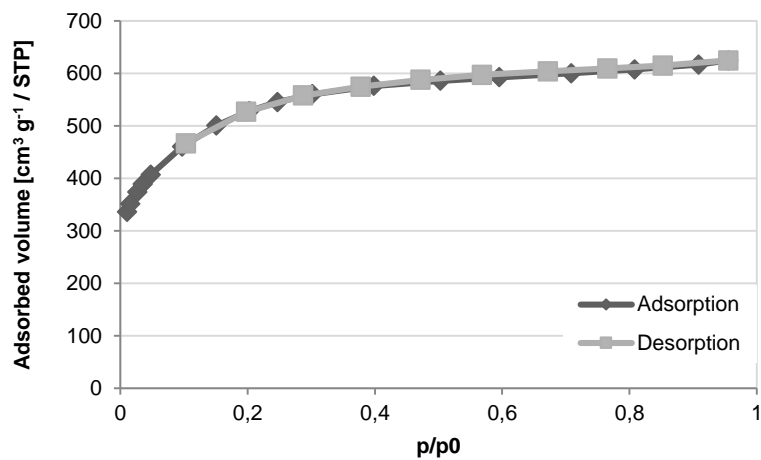


Figure S2. Nitrogen physisorption isotherm for Activated Carbon Norit A SUPRA EUR.

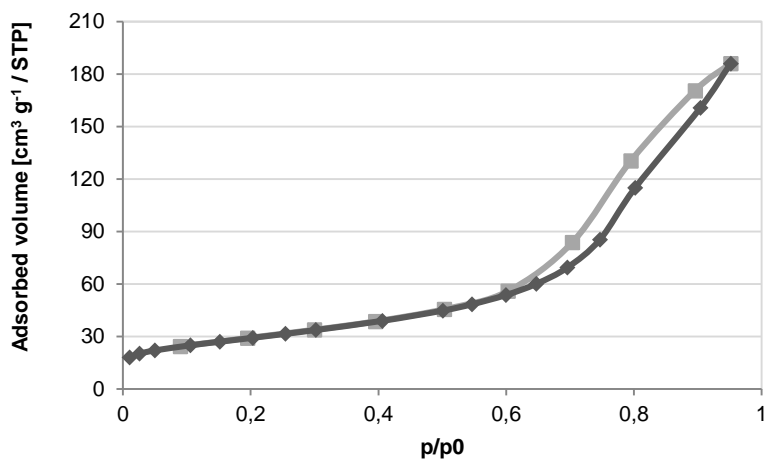


Figure S3. Nitrogen physisorption isotherm for Saint Gobain ZrO₂.

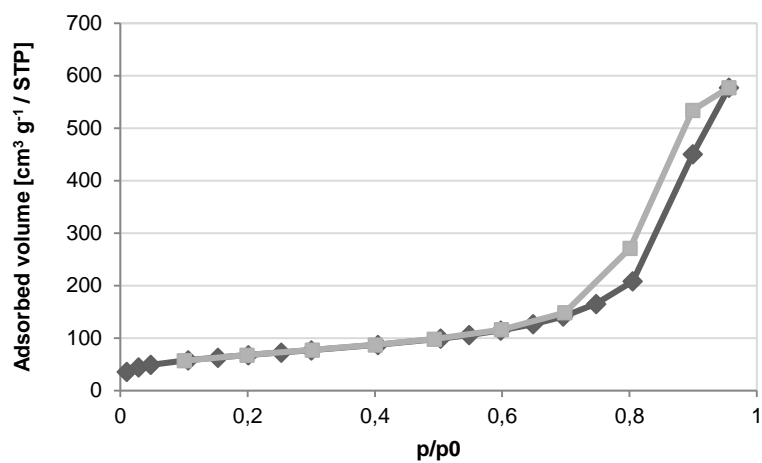


Figure S4. Nitrogen physisorption isotherm for Saint Gobain SiO₂.

Table S2. Properties of various support materials and corresponding stable catalysts determined by nitrogen physisorption.

Material	S_{BET} [m² g⁻¹]	V_P [cm³ g⁻¹]
TiO ₂	152	0.393
ReO _x /TiO ₂	137	0.340
C	1879	0.966
ReO _x /C	1634	0.912

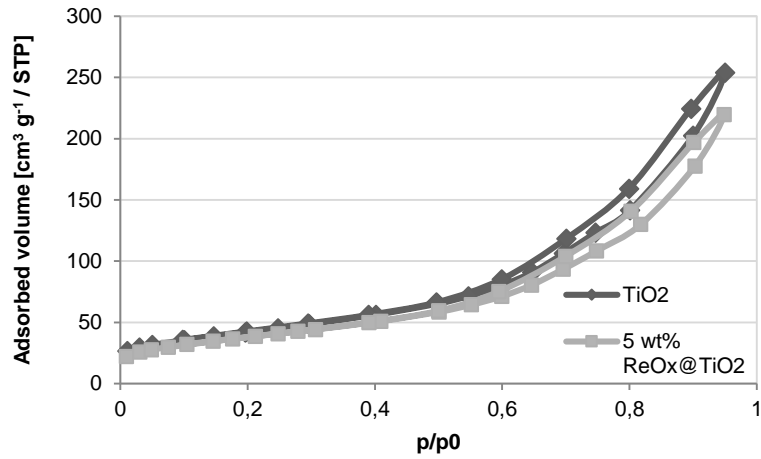


Figure S5. Nitrogen physisorption isotherms for Saint-Gobain TiO₂ and corresponding ReO_x/TiO₂.

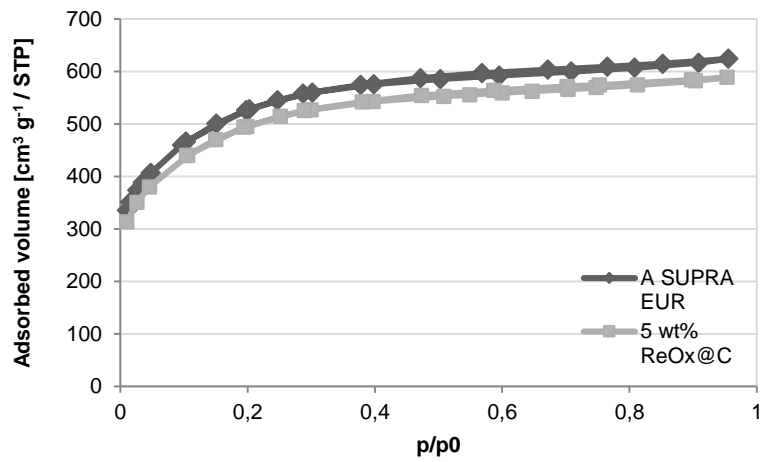


Figure S6. Nitrogen physisorption isotherms for Norit A SUPRA EUR and corresponding ReO_x/C.

3. TPR

TPR analysis was performed using a TPDRO 1100 device from CEInstruments with TCD detection. As reactive gas, H₂ (10% in Ar) was used with a flow rate of 32 cm³ min⁻¹. The sample was brought to 50 °C and steadily heated to 900 °C with a ramp of 10 K min⁻¹, held for 2 h and cooled down to 50 °C. The TPR profile of the metal precursor supported on titania is shown in figure S7. The reduction of APR/TiO₂ proceeds stepwise with a main hydrogen uptake at around 250 °C. However, the TPR profile indicates a complex reduction mechanism with further reduction steps in the temperature range of 250-500 °C indicating a strong metal support interaction.

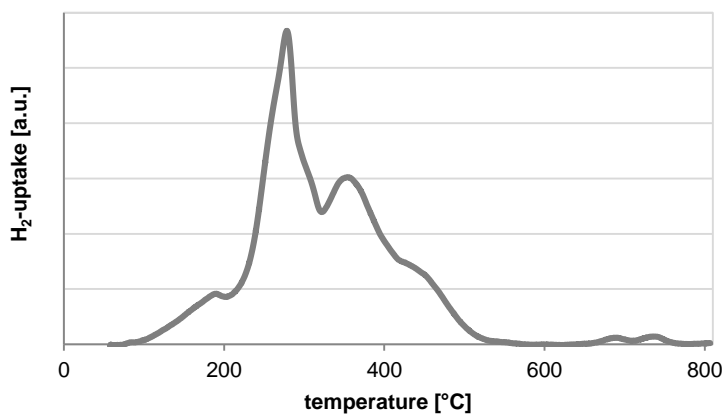


Figure S7. TPR profile of a NH₄ReO₄/TiO₂ catalyst.

4. ICP-OES Analyses

The catalysts were analysed with Inductively Coupled Plasma-Optical Emission Spectrometry (ICP-OES) using a Spectroflame device from Spectro. Samples were dissolved with either HF/H₂SO₄ or HF/HNO₃/HCl and subjected to an Ar plasma. The resulting emission spectra were collected in the range of 165-800 nm. An overview of the metal contents of the prepared catalysts is given in Table S3.

Table S3. Determination of Re metal content of prepared catalysts.

Catalyst	Re _{target} [wt.%]	Re _{found} [wt.%]
NH ₄ ReO ₄ /TiO ₂	5	5.6
ReO _x /TiO ₂	5	4.5
NH ₄ ReO ₄ /C	5	4.9
ReO _x /C	5	3.6
NH ₄ ReO ₄ /ZrO ₂	5	5.4
ReO _x /ZrO ₂	5	3.8
NH ₄ ReO ₄ /SiO ₂	5	4.8
ReO _x /SiO ₂	5	3.5

5. Hexanediol deoxydehydration

As standard reaction, 1,2-hexanediol deoxydehydration to yield 1-hexene was performed. An overview of the reaction with time resolved evolution of conversion, selectivity and yield is given in Figure S8 for $\text{ReO}_x/\text{TiO}_2$ as heterogeneous catalyst. Reactions were carried out with 1 h reaction time enabling a reasonable catalyst comparison. At long reaction times, the selectivity is decreased due to consecutive reactions or decomposition of the product.

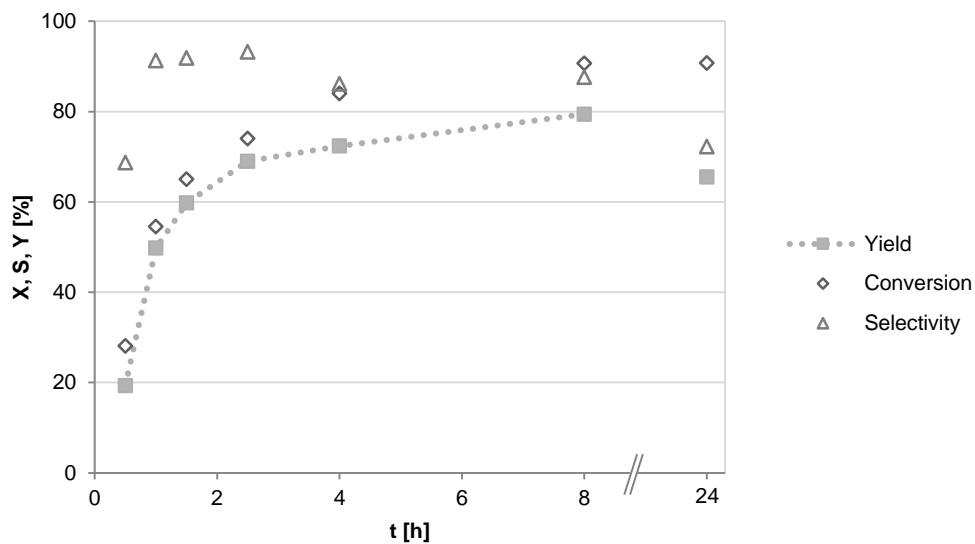


Figure S8. Reaction profile of 1,2-hexanediol deoxydehydration catalyzed by heterogeneous $\text{ReO}_x/\text{TiO}_2$.

The stability of the catalysts has been probed via recycling experiments in form of seven consecutive catalysis runs. The highlighted stability of the catalyst system $\text{ReO}_x/\text{TiO}_2$ does not only account for a constant product yield, but also for the level of conversion as shown in figure S9.

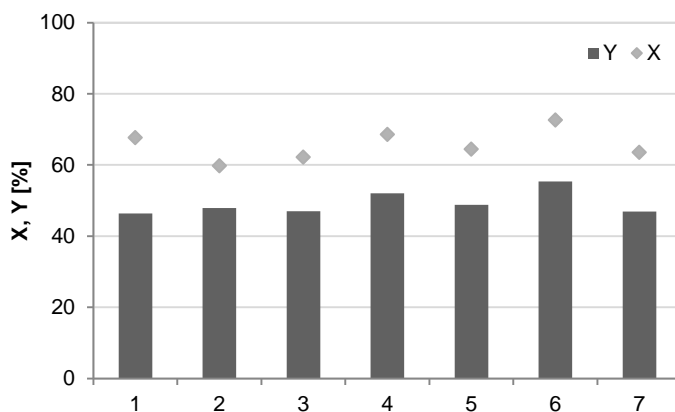


Figure S9. Recycling experiments of 1,2-hexanediol deoxydehydration catalyzed by heterogeneous $\text{ReO}_x/\text{TiO}_2$.

6. Comparison of reduction temperature for $\text{ReO}_x/\text{TiO}_2$

The reduction temperature was varied as the TPR profile showed a complex reduction behaviour with multiple uptakes. Resulting catalysts at reduction temperatures of 300, 400 and 500 °C were subjected to a recycling study. The catalysts reduced at 300 °C shows highest activity and stability, whereas the samples reduced at higher temperature are less active and show a slight deactivation over seven consecutive runs.

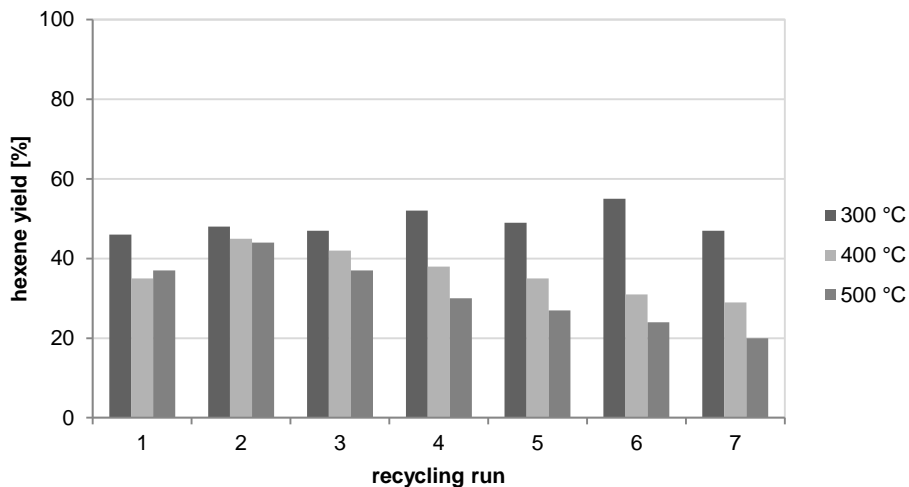


Figure S10. Comparison of activity and recycling performance of different reduction temperatures for $\text{ReO}_x/\text{TiO}_2$.

7. Recycling experiments at 190 °C

The catalyst stability of $\text{ReO}_x/\text{TiO}_2$ was also tested at a higher reaction temperature of 190 °C shown in Figure S11. Recycling of the catalyst was also feasible proving the high stability of the presented system. However, the side reaction of 3-octanol dehydration becomes more pronounced in comparison to reactions at 170 °C.

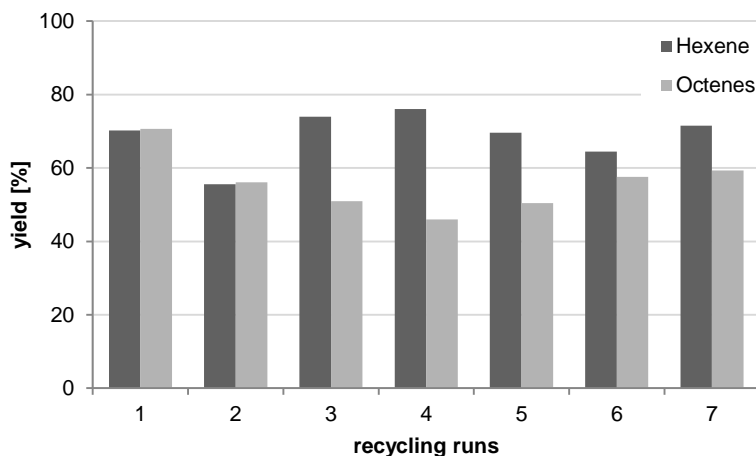


Figure S11. Recycling study of 1,2-hexanediol DODH with $\text{ReO}_x/\text{TiO}_2$, 190 °C, 1h.

8. Hot filtration test

Along with the recycling stability, a hot filtration test was performed to check for leached catalytically active species. The reaction with a $\text{ReO}_x/\text{TiO}_2$ was performed under standard conditions. Instead of cooling down the reaction mixture, the catalyst was separated through hot filtration. The filtrate was submitted once more to the standard reaction conditions. The hot filtration experiment after the first and the third run is given in Figure S12. For the first run, a slight increase in 1-hexene yield was detected due to a minor extent of leached species. The more pronounced increase in octenes yield is indicative of Re(VII) as leached species. After the third run, only negligible contribution from leached species can be detected emphasizing the stability of the catalyst, also supported by elemental analysis showing no significant decrease of metal content after catalysis.

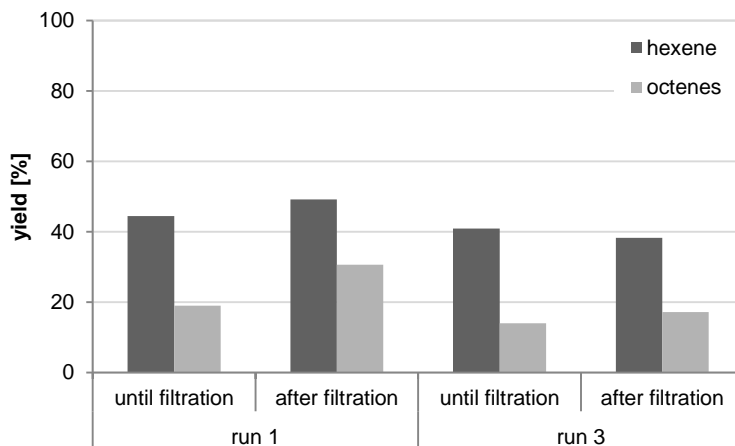


Figure S12. Investigation of $\text{ReO}_x/\text{TiO}_2$ leaching behavior by hot filtration test.

9. Mass transfer considerations

$\text{ReO}_x/\text{TiO}_2$ is an effective heterogeneous catalyst for DODH reactions. To study the effect of film diffusion and mass transport within the catalyst grain, comprehensive parameter screenings were performed shown in figures S13 and S14. The stirring speed shows only minor differences in hexene yields suggesting no significant limitations from film diffusion, especially at 700 rpm that has been used throughout the study as stirring speed. Interestingly, even without stirring, yields comparable to low stirring speeds were obtained. Concerning catalyst grain size variations, the activity increases moderately with decreasing grain sizes below $63 \mu\text{m}$ due to enhanced mass transfer. Therefore, a partial limitation for the applied catalysts can occur. However, since the fraction of particles with grain sizes lower than $25 \mu\text{m}$ is in the order of 5% of the weight for typical catalysts, the synthesized catalysts were used without further sieving of particles.

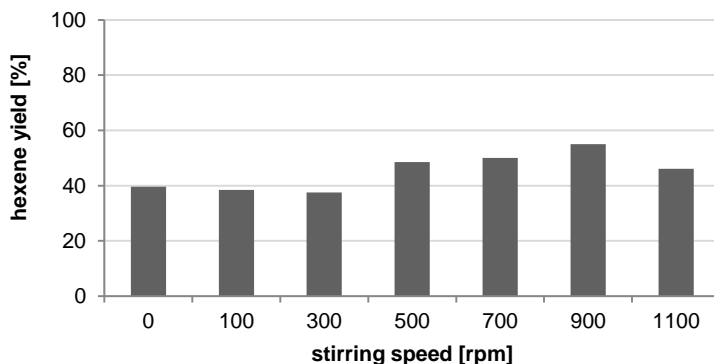


Figure S13. Variation of stirring speed in the DODH of 1,2-hexanediol, $170 \text{ }^\circ\text{C}$, 1h.

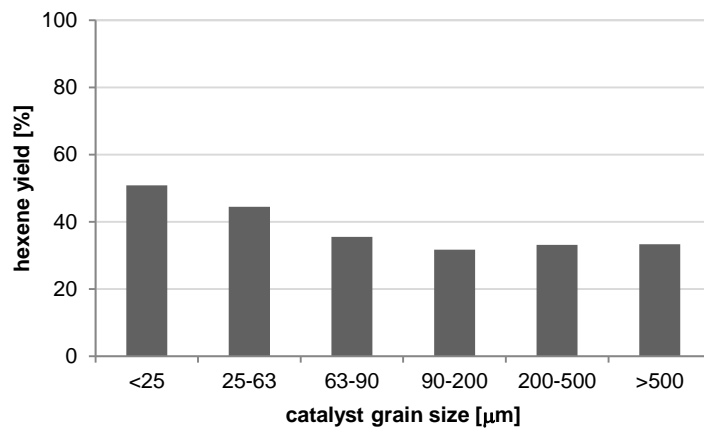


Figure S14. Variation of catalyst grain size in the DODH of 1,2-hexanediol, 170 °C, 1h.

10. Reproducibility

The promising heterogeneous catalysts were analyzed in terms of reproducibility shown in figure S15. Due to the catalyst preparation of wet impregnation and subsequent reduction, inhomogenities and therefore varying activities can arise. For the described catalysts, variations do occur between catalyst batches, however the general explained trends are not affected by this.

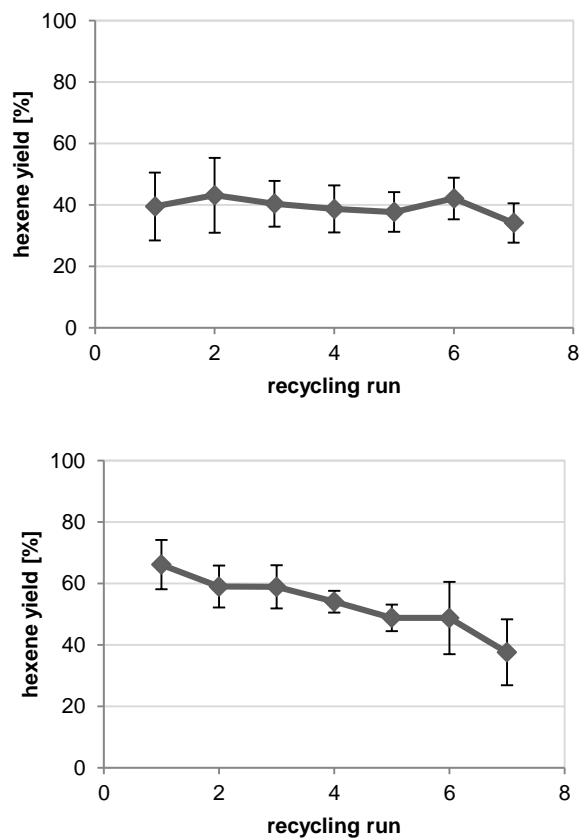


Figure S15. Recycling of ReO_x/TiO₂ (left, 4 times repeated) and ReO_x/C (2 times repeated) with corresponding error bars.

11. Application to other substrates

Apart from the model substrate 1,2-hexanediol, we sought to utilize the heterogeneous DODH catalysts for further substrates to prove general applicability of the catalysts. Triols with varying chain lengths were chosen as more challenging substrates. The recycling of $\text{ReO}_x/\text{TiO}_2$ in the DODH of these substrates is depicted in figure S16. The catalyst does transform the triols into corresponding olefins maintaining relatively constant activity over seven consecutive runs confirming the applicability of the presented catalyst system.

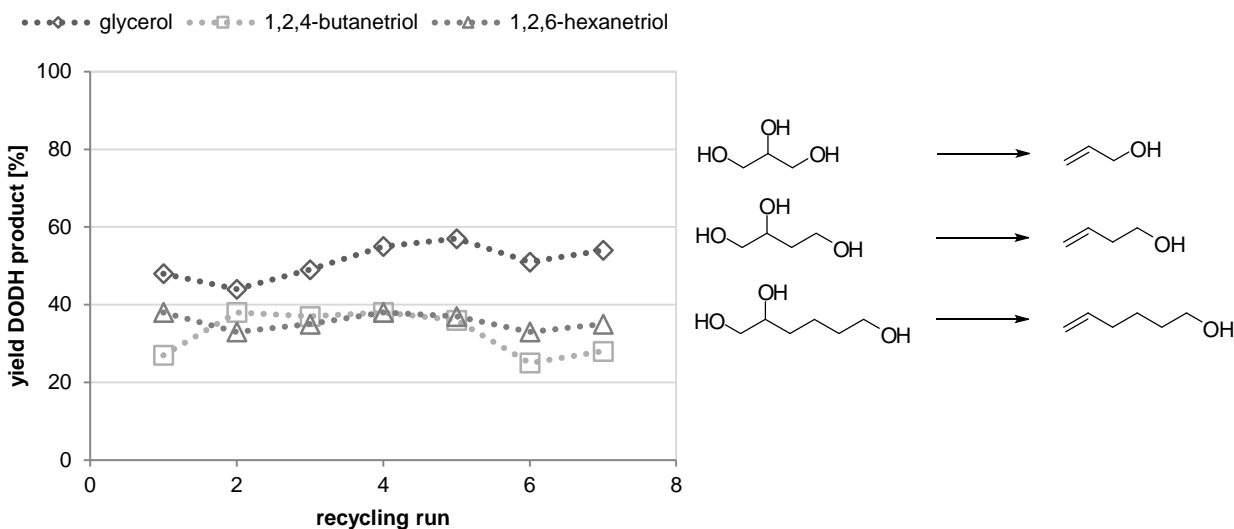


Figure S16. Recycling study of DODH of further substrates with $\text{ReO}_x/\text{TiO}_2$, 170 °C, 1h.

12. XAFS

X-ray absorption spectroscopy measurements were initially performed on station BM01B at the ESRF and subsequently on B18 at the Diamond Light Source national synchrotron facility. The stations are equipped with a Si(111)/Si(311) double crystal monochromator, and ion chambers for measuring incident and transmitted beam intensities for recording X-ray absorption spectra. The measurements were carried out using a Si(111) monochromator at the Re K-edge with the respective W monometallic foils (10 μm) used as an energy calibrant for the monochromator. Measurements were performed in quick scanning mode; the time taken for each scan was ca. 5 min (a step size of 0.5 eV and counting time of 1/6 s/point was used for collection of data around the edge). To improve the signal-to-noise ratio, multiple scans were taken. Samples were pressed into 13 mm pellets using an appropriate amount of cellulose as binder and submitted to *ex-situ* XAFS experiments. All data were subjected to background correction using Athena (i.e. IFFEFFIT software package for pre and post edge background subtraction and data normalization[1,2]). XAFS spectra were normalized from 30 to 150 eV above the edge energy, while the EXAFS were normalized from 150 eV to the last data point using the Autobk algorithm. Normalization was performed between $\mu(E)$ and $\mu_0(E)$ via a line regression through the data in the region below the edge and subtracted from the data. A quadratic polynomial is then regressed to the data above the edge and extrapolated back to E_0 . The extrapolated value of the post edge polynomial at E_0 is used as the normalisation constant. This threshold energy (E_0) was determined using the maximum in the 1st derivative. XANES spectra of rhenium reference compounds are shown in figure S17. A calibration curve (Figure S18) derived from the references was used to determine oxidation states from the edge position obtained from the maximum in the first derivative of the measured XANES spectra of the samples (figure S19).

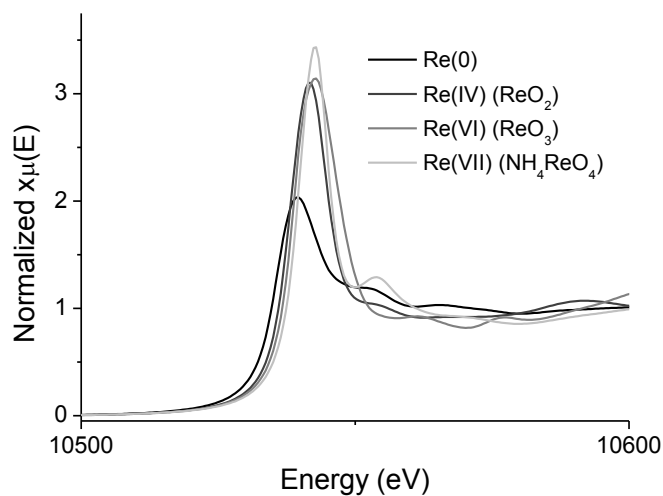


Figure S17. XANES spectra of the measured rhenium reference compounds of various oxidation states..

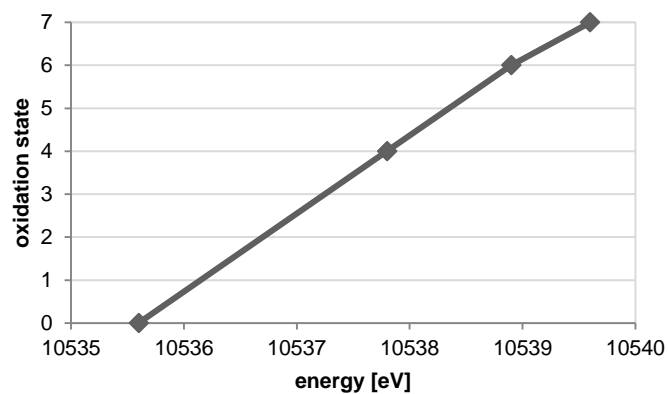


Figure S18. Calibration curve of rhenium reference compounds for determination of oxidation state.

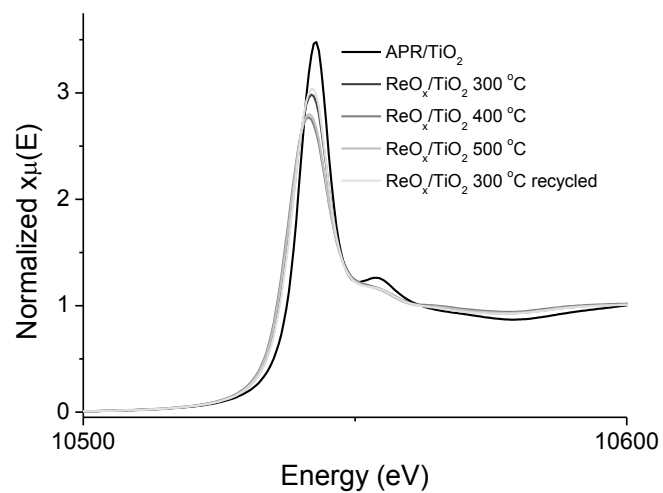


Figure S19. XANES spectra of the measured supported catalysts based on titania.

From the EXAFS features of the measured samples, a linear fitting was conducted to obtain an estimation of the composition of the found rhenium species. We note that a similar approach was previously employed by Yi et al. [3] However, an accurate determination of the maximum in the first derivative is difficult since it concerns only a small number of observations (< 10 data points) and is susceptible to noise. Thus a more reliable analysis of the sample composition could be reasonably expected from a Linear Combination Fitting (LCF) of the XANES (~ 150 data points) and EXAFS (> 500 data points) regions using Re reference compounds. However, careful consideration should be given to the effect of particle size when comparing bulk reference compounds vs. nano/atomic Re-containing samples since many of the reference compounds contain multiple scattering features in the XANES and EXAFS which are absent in the catalyst samples. In order to minimise the effects of the associated errors in the various means to determine Re composition and average oxidation state we performed a detailed LCF analysis of the XANES and EXAFS data, in the latter case, evaluated the effect of k-weighting (where $k=1-3$) on the results which are shown in Figure S20.

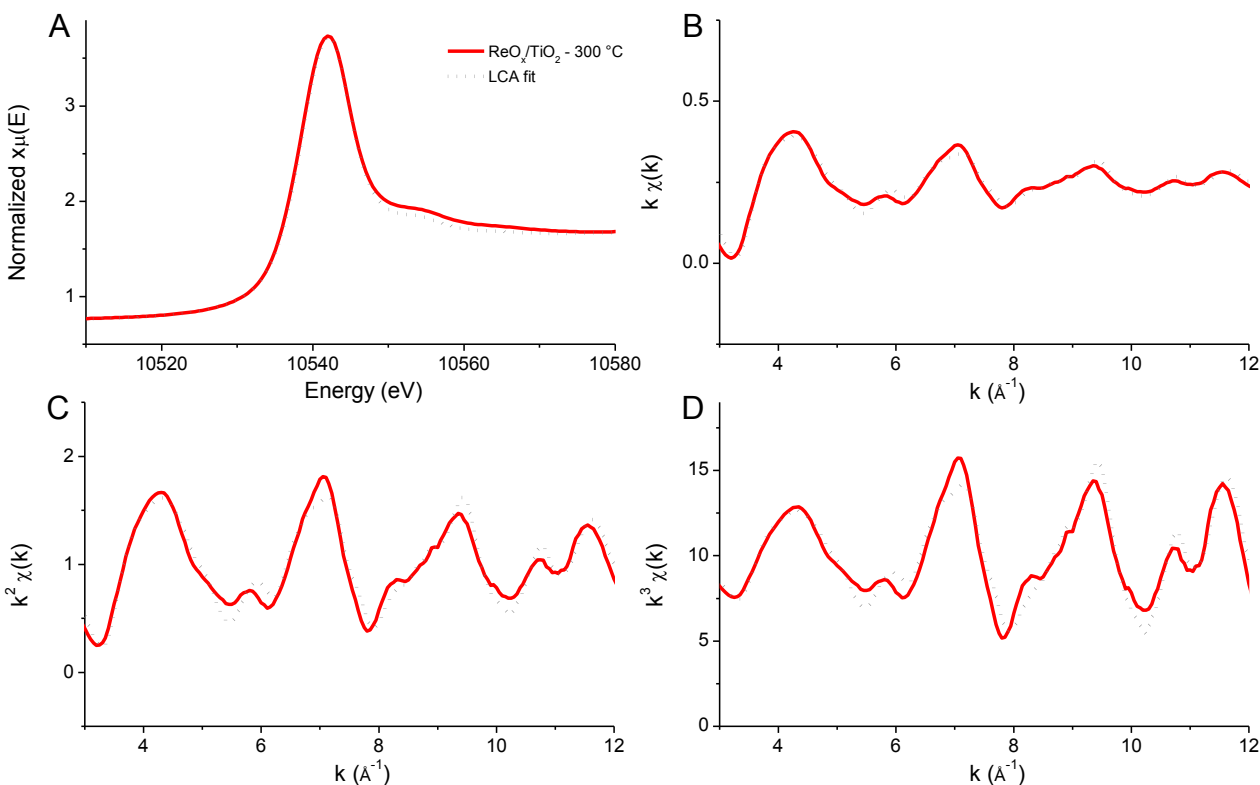


Figure S20. A. XANES, and B-D. k^1 , k^2 , and k^3 EXAFS of $\text{ReO}_x/\text{TiO}_2$ reduced at 300 °C plotted against linear combination fitting.

The purpose of LCF is to calculate, based on least squares fitting, the species present in each system in/using normalized and aligned $\mu(E)$ spectra. This method exploits the characteristic features of each standard in the XANES region as well as EXAFS region. Normally LCF is performed on XANES data, however with Re complexes, the XANES features are similar to each other whereas some features are more distinct in the EXAFS region. Note that data are constrained so that the total fraction of components is never > 1.0 . Furthermore the goodness of fit (R-factor) was determined from the expression:

$$\text{R factor} = \frac{\sum ((\text{data} - \text{fit})^2)}{\sum (\text{data}^2)}$$

A low R-factor corresponds to a better fit to the data and this is reflected in the lower values obtained for the XANES data where there are fewer data and features to fit. There is a negative correlation between the k-weighting of the

EXAFS data and the goodness of fit which can be explained by the lower signal-to-noise at high k and a likely greater mismatch between the particle sizes of the catalysts vs. the reference compounds which typically possess a more intense signal at higher k . However little difference was observed between the composition values determined as a function of k -weighting. Furthermore a good agreement was found between the E0, XANES LCF and EXAFS LCF. In terms of precision it is likely that k^1 and k^2 -weighted EXAFS data are perhaps the most reliable analyses since they contain the greatest number of data whilst at the same time are less susceptible to the differences between sample and reference data. As can be seen in Table S4, the LCF fitting for the EXAFS data is remarkably good most likely due to the EXAFS being dominated by Re speciation (i.e. little influence from the support) and suggests a more reliable approach for LCF analysis when the Z value of the absorber is much greater than that of the other elements present in the sample. A graphical overview of the goodness of the fits is given in figure S21. The k^2 -space spectra of selected reference compounds as well as the samples are depicted in figures S22 and 23, whereas the standard compounds EXAFS for fitting are shown in figure S24.

Table S4. R-factors obtained for the fitting of XANES and k^{1-3} weighted EXAFS data, with the obtained compositions shown in Figure S17.

Sample	R-factor			
	XANES	EXAFS k^1	k^2	k^3
APR/TiO ₂	0.000245	0.003	0.004	0.008
ReO _x /TiO ₂ (300 °C)	0.001391	0.035	0.065	0.094
ReO _x /TiO ₂ (400 °C)	0.037782	0.071	0.109	0.126
ReO _x /TiO ₂ (500 °C)	0.026813	0.047	0.07	0.076
ReO _x /TiO ₂ (300 °C) Recycled	0.024228	0.037	0.063	0.9

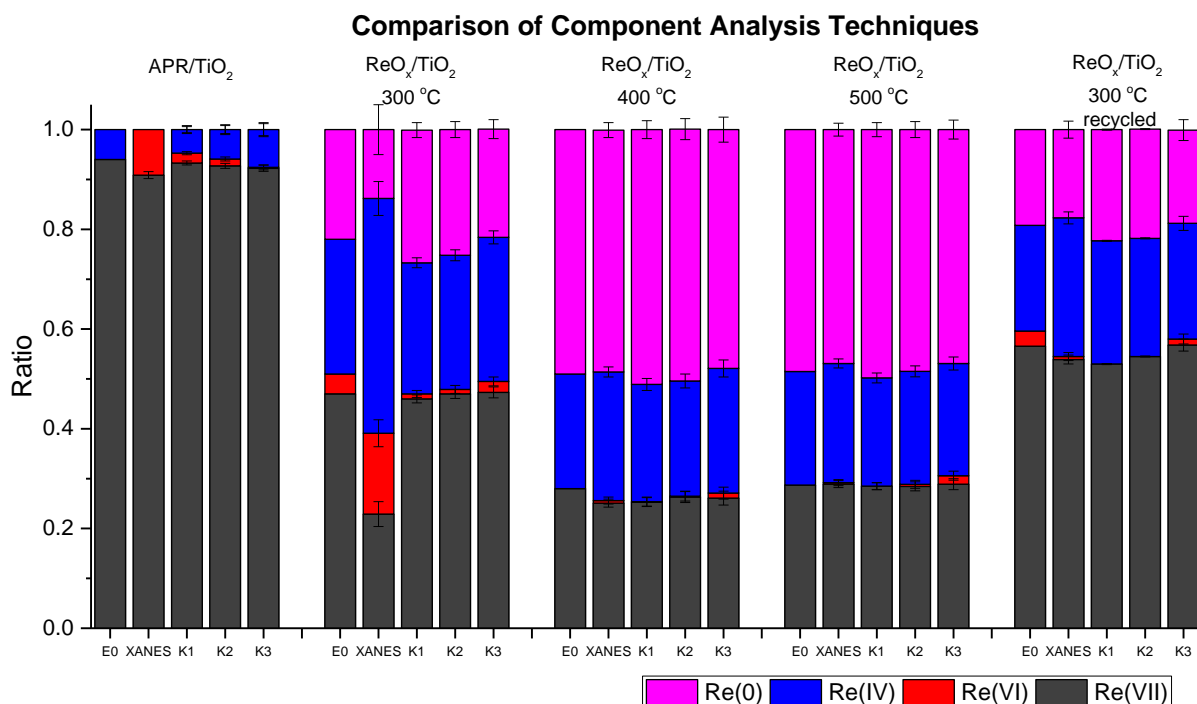


Figure S21. Estimated catalyst composition obtained from Linear Combination Fitting (LCF) of XAS data.

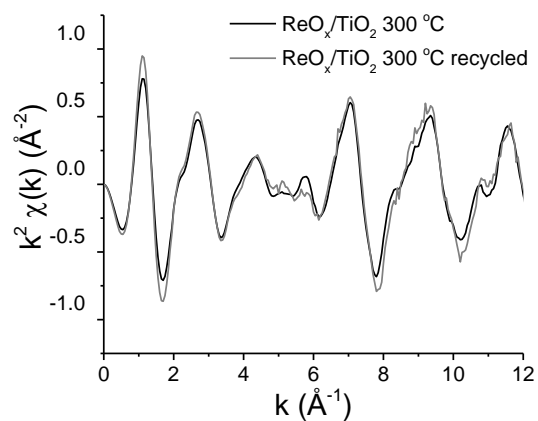


Figure S22. k^2 weighted EXAFS spectra of $\text{ReO}_x/\text{TiO}_2$ before and after catalysis.

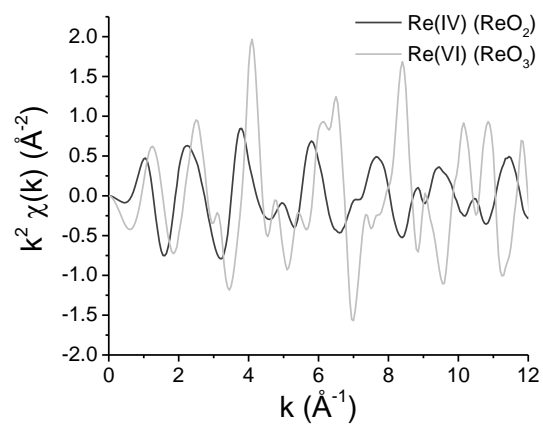


Figure S23. k^2 weighted EXAFS spectra of selected rhenium oxides.

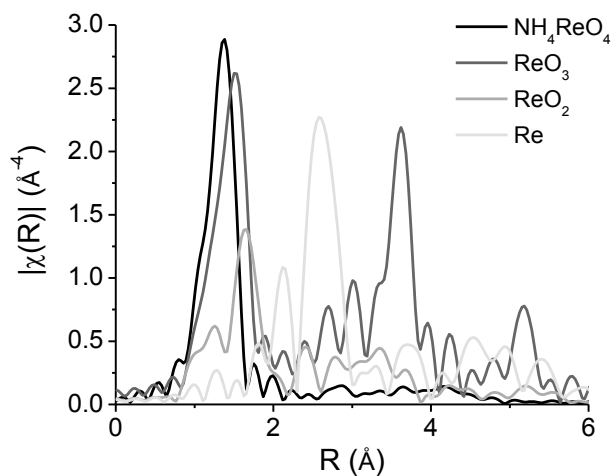


Figure S24. Fourier Transform of standard compounds NH_4ReO_4 , ReO_3 , ReO_2 , and Re .

Copies of the raw XAFS data can be obtained from the following URL: <http://tiny.cc/acscatal5b01936>

13. TEM-EDX

Electron microscopic measurements were conducted at a FEI Tecnai F20 equipped with an HAADF detector. Samples were dispersed in ethanol and transferred onto Cu round hole grids. The elemental composition and the microscopic analysis of two $\text{ReO}_x/\text{TiO}_2$ samples can be found in Table S5 and Figure S25, respectively.

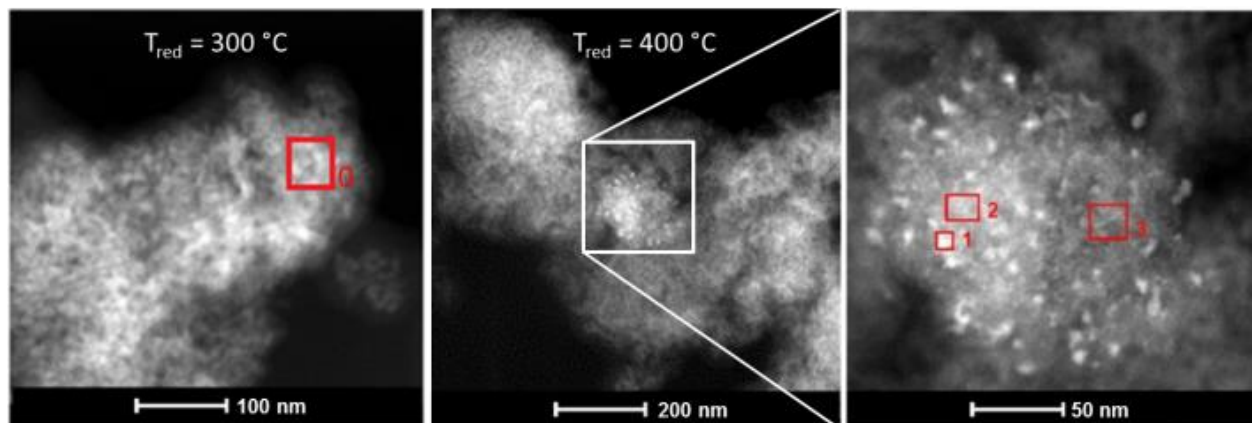


Figure S25. TEM analysis of $\text{ReO}_x/\text{TiO}_2$ reduced at two different temperatures.

Table S5. Overview of determined element masses via TEM-EDX.^[c]

Element	Mass 0 ^[a]	Mass 1 ^[b]	Mass 2 ^[b]	Mass 3 ^[b]
Oxygen	38.00	12.28	22.24	15.24
Titanium	26.81	26.62	28.27	31.01
Rhenium	3.95	47.80	16.50	15.33

[a] $T_{\text{red}} = 300$ °C. [b] $T_{\text{red}} = 400$ °C. [c] Deviations from 100% are due to Cu and Si masses.

14. References

- [1] Neville, M. J. *Synchrotron Radiat.* **2001**, *8*, 322-324.
- [2] Ravel, B.; Neville, M. J. *Synchrotron Radiat.* **2005**, *12*, 537-541.
- [3] Yi, J.; Miller, J. T.; Zemlyanov, D. Y.; Zhang, R.; Dietrich, P. J.; Ribeiro, F. H.; Suslov, S.; Abu-Omar, M. M. *Angew. Chem.* **2014**, *126*, 852-855.